frontiers | Frontiers in Environmental Chemistry

TYPE Original Research
PUBLISHED 23 October 2024
DOI 10.3389/fenvc.2024.1462678

OPEN ACCESS

EDITED BY
Zimin Li,
Institute of Earth Environment, Chinese Academy of Sciences (CAS), China

REVIEWED BY
Claudio Imparato,
University of Naples Federico II, Italy
Xiaodong Zhang,
Tianjin University, China
Xiaomin Yang,
Guizhou University, China

*CORRESPONDENCE
Jörg Schaller,
Joerg.Schaller@zalf.de

RECEIVED 11 July 2024
ACCEPTED 07 October 2024
PUBLISHED 23 October 2024

CITATION
Ellerbrock RH, Stein M and Schaller J (2024) Comparing silicon mineral species of different crystallinity using Fourier transform infrared spectroscopy.
Front. Environ. Chem. 5:1462678.
doi: 10.3389/fenvc.2024.1462678

Comparing silicon mineral species of different crystallinity using Fourier transform infrared spectroscopy

Ruth H. Ellerbrock[1], Mathias Stein[1,2] and Jörg Schaller[1,3]*

[1]Leibniz Centre for Agricultural Landscape Research (ZALF), Müncheberg, Germany, [2]Martin Luther University Halle-Wittenberg, Soil Science and Soil Protection, Halle(Saale), Germany, [3]Justus Liebig University Giessen, FB 09 Agrarwissenschaften, Ökotrophologie und Umweltmanagement, Giessen, Germany

In soils, various solid silica (Si) species exhibit different weathering behaviors and surface reactivities, which are among other characteristics related to the crystallinity of the silicate tetrahedral network. Amorphous species exhibit faster weathering and generally possess a larger specific surface area in comparison to crystalline species. However, the characterization of these different species is commonly based on wet chemical extraction methods, which lack selectivity. While Fourier transform infrared spectroscopy (FTIR) in the mid-infrared range can differentiate between short-range ordered aluminosilicates (SROAS) and pure amorphous silica (ASi), few systematic studies are found on the IR spectral features that distinguish solid Si species by crystallinity. This study aims to identify FTIR absorption bands that can differentiate Si species based on their crystallinity. Our data clearly indicate that ASi can be distinguished from very crystalline silica (quartz) and sea sand. The absorption band at approximately 800 cm^{-1} in the FTIR spectra allows determining the degree of crystallinity of the studied ASi species since the band becomes smaller and the band maximum shifted toward lower wavenumbers with increasing degree of crystallinity. Hence, FTIR spectra may be used to differentiate certain Si species in complex samples like soils, allowing the estimation of weatherability and surface reactivity of those species.

KEYWORDS

FTIR, amorphous silica, minerals, crystallinity, short-range ordered aluminosilicates, analysis of soil composition, soil silicon

1 Introduction

Growing evidence suggests that silica (Si) can have a significant impact on ecosystem processes such as nutrient availability, water retention (Schaller et al., 2020), and crop productivity (Katz et al., 2021; Schaller et al., 2023), as well as ecological cycles (Schaller et al., 2021). However, for those effects, several forms of Si are relevant. In terrestrial environments, silicon occurs in a variety of solid compounds including crystalline minerals (e.g., quartz and feldspars), short-range ordered species (e.g., imogolite and allophanic minerals), and amorphous silica of biogenic or minerogenic origin. The weathering of these solids releases dissolved silicon into the solution and strongly differs between these minerals (Schaller et al., 2021). In solution, silicon exists in a dynamic equilibrium of monomeric and polymeric silicic acid controlled by solution pH, silicic acid concentration, and ionic

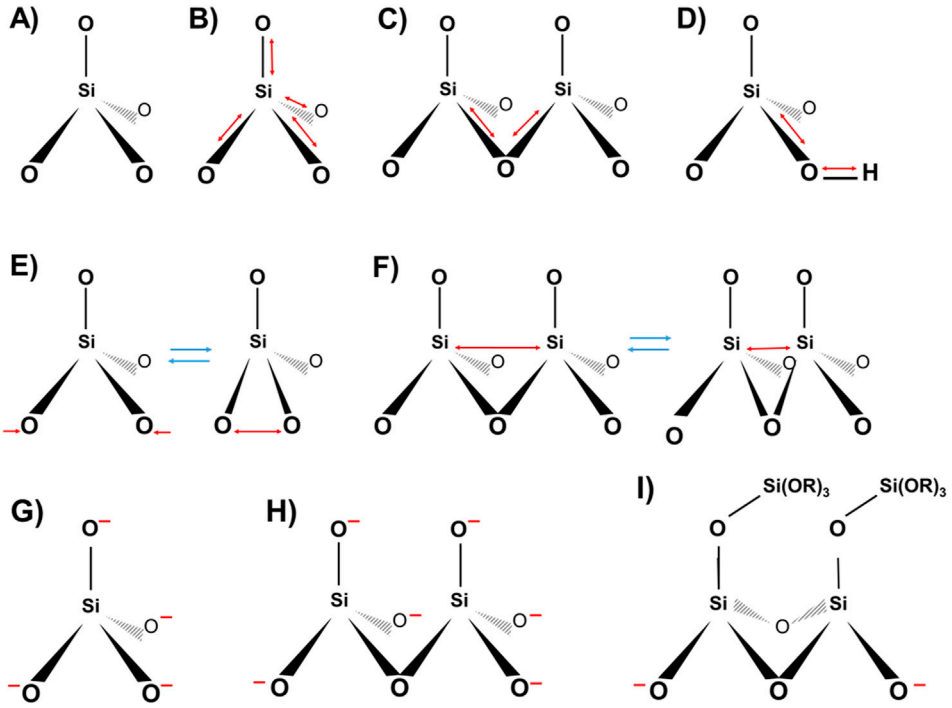

FIGURE 1
(A) SiO_4 tetrahedral structure and potential vibration modes within the Si-O-Si bonds, **(B)** internal Si-O stretching within the tetrahedron, **(C)** intra-Si-O stretching along Si-O-Si bonds with the O bridging two tetrahedra, **(D)** O-H stretching in the SiO_3OH tetrahedron, **(E)** internal O-Si-O bending, and **(F)** intra bending modes of the Si-O-Si bond, as suggested by Fröhlich (2020) as well as schemes indicating the negatively charged oxygen atoms in **(G)** a silicate monomer, **(H)** a silicate dimer, and **(I)** a silicate polymer.

strength of the solution (Dietzel, 2002). The differences in weatherability among various forms of silica, originating from factors such as crystallinity and specific surface area, necessitate their distinct identification in terrestrial samples. Therefore, analytical methods are required to characterize Si species that differ in crystallinity and potentially enable quantification. However, the common analytical methods that are based on wet chemical extraction procedures are not entirely selective, and thus an exclusive quantification of the target Si species alone remains elusive (Stein et al., 2024). The term crystallinity is used to describe the degree of regularity of the silicate tetrahedron network (regular and periodic arrangement). The crystallinity increases from amorphous via short- toward long-range ordered silicates (Liu et al., 2022).

More recently, Fourier transform infrared spectroscopy (FTIR) analyses were successfully applied to distinguish between short-range ordered aluminosilicates (SROAS) and pure amorphous silica (ASi) (Ellerbrock et al., 2022). Other studies indicate the difference between quartz sand and ASi like glasses (McMillan and Piriou, 1983; Liu et al., 2022), the latter by using Raman spectroscopy. Additionally, Gunde (2000) interpreted FTIR data by using energy-loss functions to determine crystal symmetry-based vibrational modes of ASi species and quartz. However, few systematic studies are found on the relation between infrared (IR) spectral features and how they can be used to differentiate between solid Si species differing in the crystallinity of the Si tetrahedral network.

In the SiO_4 tetrahedron (Figure 1A), various stretching and bending modes can be excited by infrared light. These modes can roughly be distinguished into bond compression/extension (Figures 1B–D) modes and bond angle deflection modes [Figures 1E, F; Gottwald and Wachter (1997); Hesse et al. (2005)], which can appear asymmetric or symmetric.

If SiO_4 tetrahedrons are part of a larger Si network comprising irregular or regular arrangements of the Si tetrahedral units, slightly different energies are required for the valence/deformation vibrations induced by IR light (Ren et al., 2017; Liu et al., 2022). Consequently, most of the absorption bands appear at different wavenumbers (WNs) depending on the degree of crystallinity of the silicates (Laudisio et al., 1998; Ren et al., 2017; Liu et al., 2022). Note that in spectra of mineral mixtures, the absorption bands of individual components behave additively (Gottwald and Wachter, 1997). Additionally, differences caused by the degree of crystallinity may be utilized for silica species that show characteristic FTIR spectral features to potentially estimate the proportion of these different species (here different in the crystallinity) in mixtures, as described by Ji et al. (2009) for dolomite or by Ichikawa et al. (2022) for crystalline silica in workplace air. Characteristic bands in FTIR spectra are, for example, usable for quantifying the amount of quartz particles (DGUV-213-582-2016 2015).

FTIR spectra of minerals like opal and quartz as well as those of volcanic glasses like obsidian showed specific absorption bands reflecting differences in the crystallinity of the Si species (Banerjee, 1993; Laudisio et al., 1998). The most significant spectral regions regarding Si and their accompanying shoulders (1,200–1,000 cm^{-1}) are attributed to internal, asymmetric stretching vibrations of Si-O-Si (ν Si-O). A broadening of this envelope may

TABLE 1 Assignment of the absorption bands in the WN region from 1,200 to 400 cm^{-1} in FTIR spectra of different silica, glasses, and soil minerals toward defined stretching and bending modes. The bold letters indicate the WN range of each band in total, and the normal letters indicate the WN range of that band for specific Si species (like glasses).

WN region; cm^{-1}	Assigned group	Remark
1,200 to 1000	ν Si-O: internal Si-O/asymmetric stretching	Most intense band
1,088	*For quartz*	Banerjee, (1993)
1,100	*For opal (i.e., hydrated amorphous form of silica)*	Hernández-Ortiz et al. (2015)
1,040–1,110	*For glasses*	Gucsik et al. (2004)
500–450	δ Si-O: internal O-Si-O bending	Varies with crystallinity (Farmer, 1974)
800–740	ν Si-O-Si: intra Si-O-Si/symmetric stretching	Si-O-Si bonding angle varies significantly with the degree of crystallinity (Liu et al., 2022)
800–790	For *soil minerals*	Farmer, (1974)
769–745	For *glasses*	Gucsik et al. (2004)
620 & 385 two bands	δ $Si\text{-}O_{crist}$: Si-O-Si in cristobalite	Missing in spectra of opals (Šimon and McMahon, 1953; Wilson, 2014)
797 & 778 one band with two maxima	δ $Si\text{-}O_{quartz}$: Si-O-Si in quartz	Banerjee, (1993)

TABLE 2 Silica studied by FTIR spectroscopy (own measurements), their description, specific surface area (SSA, $m^2\ g^{-1}$), pH values of suspension in water (pH/% silica per 100 mL of water), weight loss on drying at 105°C for 2 h (loss; %), and SiO_2 content (SiO_2; %) as well as origin or reference.

Si-O species	Description	SSA *(BET)*	pH/ SiO_2	Lost	SiO_2	Origin/references
	-	$m^2\ g^{-1}$	-/%	%	%	-
Quartz sand (ground <10 μm)	Crystalline silica; SiO_2	3.5[A]	6.5/20	<4	>90	Quartzwerke Weferlingen, Germany (Meloni et al., 2012)
Sea sand (ground <10 μm)	Heated crystalline silica; SiO_2	3.5[A]	6.5/20	<4	>90	Roth, Germany
Silica gel (ground <10 μm)	Pyrogenic silica; SiO_2	750–800[B]	-	<4	>90	Merck, Germany (Christy, 2008)
Amorphous silica						
Sipernat 320	Precipitated silica, SiO_2	180	6.2/4%	<7	97	Evonik
Aerosil 300	Pyrogenic silica; SiO_2	270–330	3.7–4.5/4%	1.5	99.8	Evonik
Phytolite	Biogenic silica; SiO_2	290–400	6/4%	<2	>90	Puppe and Leue (2018)

account for a lower internal order of the Si species (Stein et al., 2020). In case of SiO_4 tetrahedra units bearing uniform Si-O bonds —forming a threefold axis of symmetry along each Si-O bond— FTIR spectra will show a relatively sharp ν Si-O band of high intensity. However, the symmetry of the tetrahedron is disrupted when the oxygen (O) atoms in the Si-O bonds of the SiO_4 tetrahedra serve as bridges to another SiO_4 unit (bridging oxygen; Figures 1H, I) or interact with a hydrogen atom or another oxide unit (non-bridging oxygen; Figures 1A, G). In turn, the ν Si-O band in FTIR increases with a decrease in the intensity (Laudisio et al., 1998). In general, the intensity of the absorption bands is related to the amount of the sample [Beer–Lambert law; Gottwald and Wachter (1997)]. For most Si-O species, the ν Si-O absorption band between 1,200 and 1,000 cm^{-1} is the most intense. In silica with a uniform SiO_4 tetrahedral network, this band appears within a narrow wavenumber range, allowing it to be used as an internal reference for comparison. The ratio between the ν Si-O-Si (quartz) band and the ν Si-O band in a mineral mixture can indicate, for example, variations in quartz content. The intensity of the bands can be quantified by measuring the vertical distance from the peak of each band to the global baseline, using the height of the band maxima, as described by Kaiser et al. (2008) for the specified regions in Table 1. Calibration by using known mixtures should allow quantifying the quartz content in the mixtures. The band at 450 to 500 cm^{-1} is assigned to Si-O bending vibrations (δ Si-O) within the Si tetrahedron (Van der Marel and Beutelspacher, 1976; Laudisio et al., 1998). The WN of the δ Si-O band maximum is affected by the tetrahedral O-Si-O bonding angle, and such varies between 470 and 487 cm^{-1} with the type of the silica crystallization [Table 1, e.g.; Farmer (1974); Van der Marel and Beutelspacher (1976)]. The δ Si-O band maximum is shifted toward lower WN in the FTIR of QS (464 cm^{-1}) that shows a higher degree of crystallinity (Liu et al., 2022). In a comparable manner, the WN of the ν Si-O-Si band maxima (assigned to the asymmetric Si-O stretching mode of bridging O) depends on the Si-O-Si bonding angle such that it also varied significantly for the different silica species of (soil) minerals

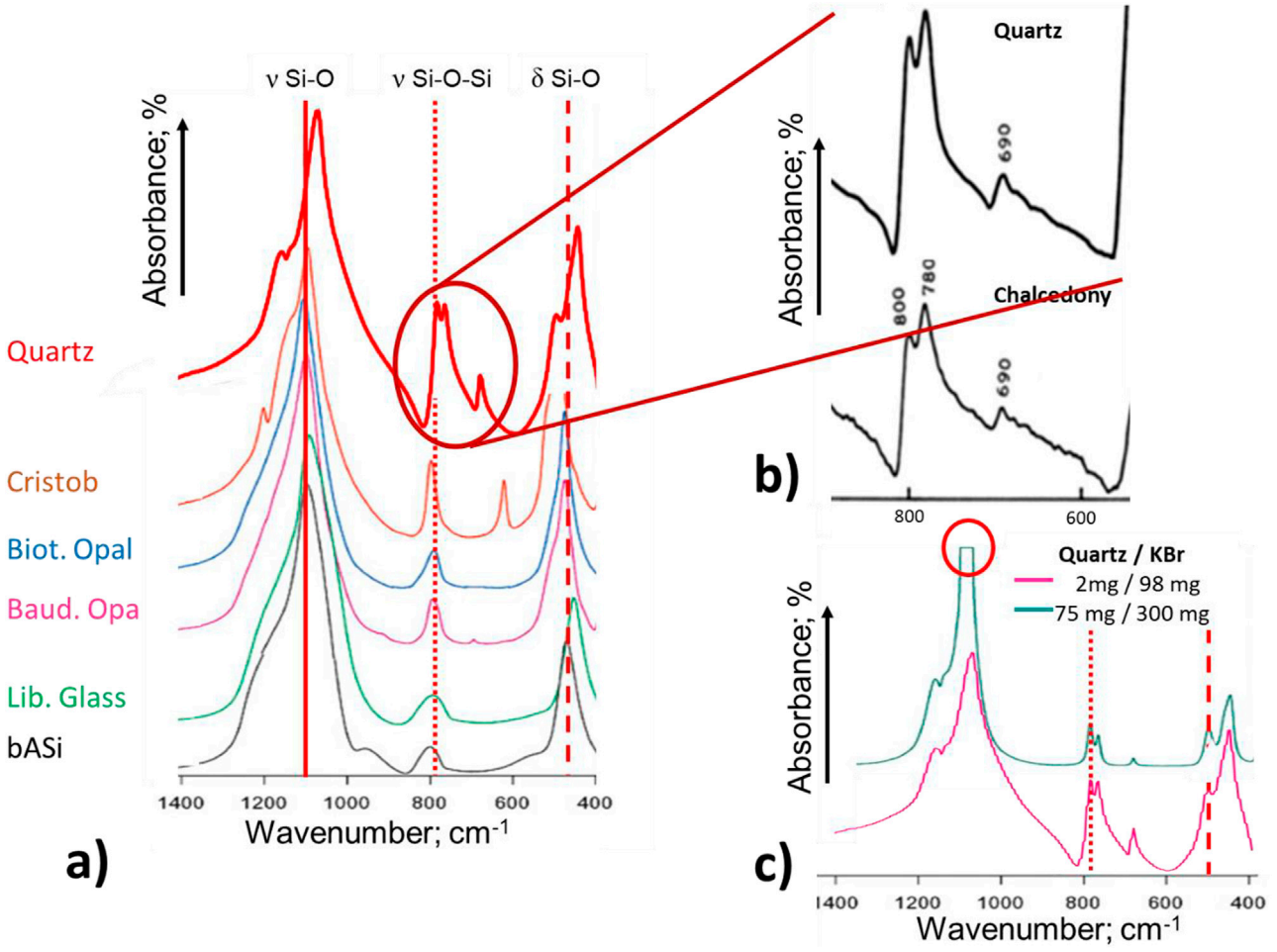

FIGURE 2
WN 1,300 to 400 cm^{-1} in FTIR spectra of finely ground quartz, synth. Cristobalite (Christob)*, biotic Opal CT (Biot. Opal)*, Baudres Opal (Baud. Opal)*, Libyan desert glass (Lib. Glass)*, and biogenic amorphous silica (bASi)*, **(B)** WN region 900 to 420 cm^{-1} in FTIR of quartz (QS enlarged region of **(A)**: reddish line at the top), compared to spectra of QS and Chalcedony shown earlier by Banerjee (1993), and **(C)** comparing the FTIR of quartz–KBr mixtures with 75 mg in 300 mg KBR* and 2 mg in 98 mg KBr. *: adapted from Fröhlich (2020).

[791–806 cm^{-1}; e.g., Fröhlich (2020)] or glasses [745–769 cm^{-1}; Gucsik et al. (2004)].

In this study, we aimed to identify specific absorption bands in FTIR spectra that can differentiate between Si species with different degrees of crystallinity.

2 Material and methods

2.1 Fourier transform infrared analyses

The Sipernat 320 and Aerosil 300 samples were used as provided by the manufacturer (white powders with particle sizes between 2 and 10 μm). These commercially amorphous silicas were chosen as they are derived from different types of synthesis. Given their relatively high specific surface area, these materials may also serve as a potential source of silicon in soil when used as a fertilizer. All samples (Table 2) were gently ground by hand in an agate mortar for approximately 5 min to obtain a powder (particle sizes between 2 and approximately 10 μm) and subsequently analyzed using an IS20 FTIR spectrometer (Thermo Fisher Scientific, Dreieich, Germany). Briefly, 2 mg of the sample (quartz, sea sand, and mixtures of quartz with ASi) was mixed with 98 mg of KBr and finely ground by hand in an agate mortar. The mixtures were dried for 12 h over silica gel in a desiccator to standardize the water content and were then pressed into pellets. The obtained KBr pellets of the minerals were analyzed in the transmission mode. All spectra were recorded in three replicates at a resolution of 1 cm^{-1} and 16 scans [=16 repetitions of a single spectra; Ellerbrock et al. (1999)] to obtain the absorption spectra in a range of wavenumbers between 4,000 and 400 cm^{-1}. All spectra were corrected against atmosphere as a background (Haberhauer and Gerzabek, 1999), smoothed using box-car function (factor 55; Bio-Rad Winirez software), and baseline-corrected.

2.2 Interpretation of FTIR spectra

The baseline-corrected spectra (Ellerbrock et al., 1999) were analyzed for the WN and the intensity of absorption bands

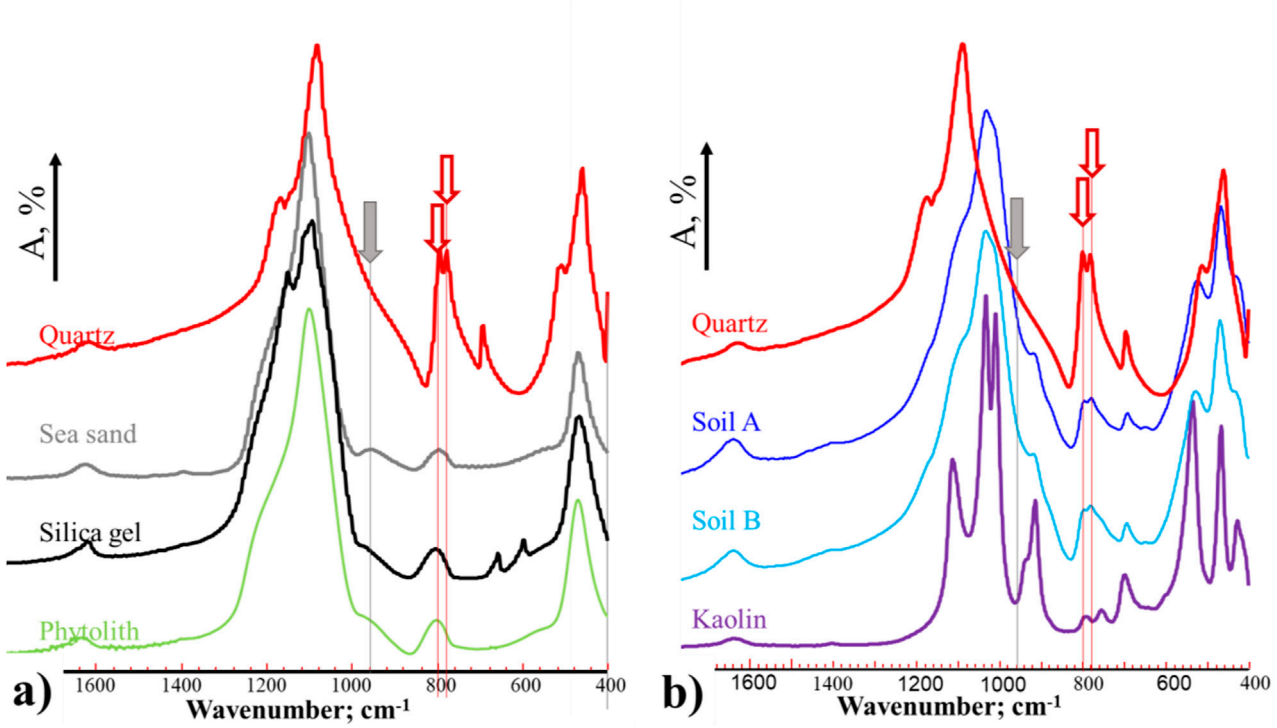

FIGURE 3
FTIR in the WN region from 2,000 to 400 cm^{-1} of finely ground quartz sand (Quarzwerke Weferlingen, Germany) compared with **(A)** silica gel, a phytolith (Puppe and Leue, 2018), and sea sand (Roth) and with **(B)** soil A (Holzendorf; Ellerbrock et al. (2016), soil B [Simmringen; Kaiser et al. (2016)], and kaolin (Rosenthal).

characteristic for stretching and bending modes in the SiO_4 tetrahedra. The characteristic absorption bands are caused by (1) internal asymmetric Si-O stretching vibration appearing at WN 1200–1,000 cm^{-1} [ν Si-O (Banerjee, 1993; Gucsik et al., 2004; Hernández-Ortiz et al., 2015)], (2) symmetric Si-O stretching vibration (with the O bridging two SiO-tetrahedra) at WN 800 to 740 cm^{-1} [ν Si-O-Si (Farmer, 1974; Gucsik et al., 2004; Liu et al., 2022)], and (3) O-Si-O bending vibrations at WN 500 to 450 cm^{-1} [δ Si-O; Farmer (1974)]. When interpreting the spectra, we focus on ν Si-O, ν Si-O-Si, and δ Si-O bands which were assumed to be mostly affected by difference in the crystallinity of the studied Si species (Farmer, 1974; Liu et al., 2022). The maxima of ν Si-O, ν Si-O-Si, and δ Si-O bands were identified using an automated identification procedure of the Bio-Rad Winirez software (Bio-Rad Corp, Krefeld, Germany) as follows: the left and right limits of the WN region characteristic for each band (Table 2; and references cited therein) were used to construct so-called "def"-files (offered by Winirez) that were then applied within the automated Bio-Rad Winirez procedure. The band of the hydroxyl groups at WN 3500 to 3,350 cm^{-1} (O–H band) was not interpreted since the shape and intensity of the O–H band are affected by O-H groups present in soil minerals and water.

In FTIR spectra of soil samples, the band at WN 3700 to 3,000 cm^{-1} is affected by OH groups of different soil constituents (e.g., oxides/hydroxides of iron or manganese, water, clay mineral, and organic matter). The bands of the different OH groups are overlapping and are affected by the formation of hydrogen bridges (Hesse et al., 2005). In consequence, they are hard to assign to these specific soil constituents in FTIR spectra of soil samples because of this and since treatments to destroy organic matter or to remove iron oxides may affect the structural aspects of the silica. Hence, we focus on Si-O bands that show a lower tendency of overlapping.

3 Results and discussion

Our data clearly demonstrate that FTIR spectroscopy can be used effectively to differentiate between crystalline silica, such as quartz, and amorphous silica. The FTIR spectra of the finely ground quartz sand (QS) (red line in Figure 2) are in accordance with the one published by Banerjee (1993). While compared with the data published by Fröhlich (2020), the intensity of ν-Si-O and δ Si-O-Si bands seems to be lower for the QS we studied (Figure 2 red circle). Such differences in band intensity can be explained by differences in QS weight within the KBr pellet. Here, we used 2 mg per 100 g KBr, while Fröhlich (2020) used 75 mg per 300 mg KBr. Because of the high QS content in the KBr pellet, the Si-O-Si band in the QS FTIR spectrum of Fröhlich (2020) shows an oversaturation of the detector [red circle in Figure 2C; see also Hesse et al. (2005)].

Note that the FTIR of sea sand (SeaS; Roth company; Figure 3A: gray line) as well as the silica gel and the phytolith did not show the double band at approximately 799 cm^{-1} which was found in the FTIR of QS. Additionally, the WN of the ν-Si-O band maximum found for QS (1,088 cm^{-1}) is shifted by approximately 20 cm^{-1} to higher WN for the SeaS (1,115 cm^{-1}; Figure 3A and Table 3).

TABLE 3 WN (cm^{-1}) of absorption bands in FTIR of opal, quartz, obsidian, and chalcedony (from Banerjee, 1993), as well as of biotic Opal CT, Baudres Opal, Libyan glass', cristobalite, and biogenic amorphous silica (Fröhlich, 2020). Bold letters indicate the WN of a band maximum, and italics letters indicating the WN of a shoulder.

	ν *Si-O*		δ Si-O-H	ν Si-O-Si			δ Si-O	References
SeaS-RE	**1,115**		**912**	**800**	-		**460**	Own findings
Quartz; <20 µm	*1,169*	**1,084**		**794**	**778**	**693**	**460**	Own findings
Quartz		**1,088**		**799**	**780**	**694**	**464**	Fröhlich, (2020)
Cristobalite		**1,099**		**802**		**621**		DGUV-213-582-2016 (2015)
Biot opal/OPAL-CT	**1,103**			**791**			**475**	Fröhlich, (2020)
Phytolith		**1,100**	*960*	**793**			**469**	Puppe and Leue (2018)
Baudres OPAL-CT		**1,099**		**794**			**475**	Fröhlich, (2020)
Opal-A		**1,096**		**800**			**470**	Fröhlich, (2020)
Synth Cristobalite		**1,089**		**797**			**487**	Fröhlich, (2020)
OPAL	**1,116**				**780**			Banerjee, (1993)
Chalcedony				**800**	**780**			Banerjee, (1993)
Desert glass	**1,102**			**806**			**472**	Fröhlich, (2020)
Obsidian		**1,088**						Banerjee, (1993)
Silica gel	**1,154**	**1,096**	*984*	**804**				Own findings
Sipernat 320		**1,090**	**962**	**799**			**465**	Own findings
Aerosil 300	*1,169*	**1,097**		**805**			**465**	Own findings
BaSi (phytolith)		**1,100**		**800**			**468**	Own findings
Quartz + phytolith	*1,169*	**1,090**		**794**	**774**	**688**	**510**	Own findings

This finding suggests that the crystallinity of SeaS (Roth) differs from that of QS, potentially due to the pretreatment process applied to SeaS. The SeaS was treated with HCl to remove carbonates and heated to 1,000°C to eliminate organic matter. This heating, in particular, may alter the structural arrangement of the SiO_4 units in this sand, leading to a more glass-like structure. This assumption is in accordance to the fact that the FTIR spectra of the SeaS are relatively similar to those of the Libyan desert glass (Figure 2, greenish line) shown by Gucsik et al. (2004). This aligns with the findings of Banerjee (1993), who observed that the shape and intensity of the peaks between 800 and 780 cm^{-1} in the IR/FTIR spectra gradually change from quartz to obsidian (glass) as crystallinity decreases in the following order: quartz > chalcedony > opal-CT > opal-A >> obsidian (volcanic glass). In addition to that, with the change in intensity, a systematic shift is noted for the ν-Si-O band maximum from 1,088 cm^{-1} for quartz to 1,160 cm^{-1} for Libyan Desert glass (Table 3; Fröhlich (2020). Note the characteristic absorption bands at WN 630 to 610 cm^{-1} described for cristobalite (Wilson, 2014, DGUV-213-582-2016 2015; Hernández-Ortiz et al., 2015) were absent in the FTIR spectra of opal, biogenic amorphous silica (bASi), and finely ground quartz sand (Figure 2) and also in the FTIR spectra of amorphous silica (ASi, Aerosil 300, and Sipernat 320) or phytolith (Figure 4).

To provide the context for the recorded spectra of silica in comparison with soil samples, we incorporated the spectra of two distinct soils shown in Figure 3B. The spectra of these soil samples also display the characteristic double band at a wavenumber of approximately 799 cm^{-1}, albeit with reduced intensity. This attenuation can be attributed not only to the presence of quartz but also to organic matter and other inorganic components within the soil, which interfere with and diminish the strength of the target signal (Kaiser et al., 2016). It is also observed that the shape of the band at wavenumbers 1,200–1,000 cm^{-1} (ν Si-O) in quartz differs from that in the soil samples. The quartz band is notably sharp and steep, whereas the bands in the soil are broader and more rounded. This suggests the possible presence of different silica species in the soils. Stein et al. (2020) demonstrated that the broadening of this band could be attributed to a decrease in the internal order, i.e., a reduction in crystallinity. This highlights the potential of this method for differentiating silica forms based on their structural characteristics.

According to Fröhlich (2020) and references therein, the FTIR of bASi exhibits an additional band at 950 $cm^{-1,}$ which is assigned to Si-OH bonds (Figure 4, brownish circle). The spectra of Sipernat (dark gray line in Figure 4) like the spectrum of bASi [black line in Figure 2 Fröhlich (2020)] show Si-OH absorption bands at differing WN 972 and 962 cm^{-1}, respectively. However, for biogenic Opal (Figure 2) and Aerosil (Figure 4), the Si-OH band is missing in the FTIR spectra. The absence of Si-OH bands in FTIR of Aerosil is caused by its synthesis by pyrolysis, resulting in surfaces poor in OH groups. The weak band at approximately 950 cm^{-1} in the FTIR spectra of finely ground SeaS (Figure 3A blue arrow) can be explained by its small particle size. With decreasing particle size, the surface area increases, thereby increasing the number of Si-O

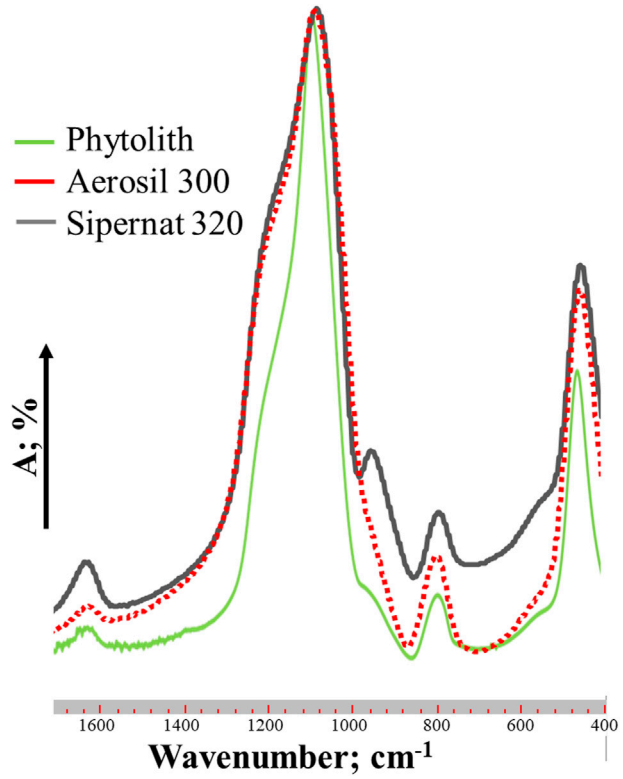

FIGURE 4
Wavenumber region from 1,800 to 400 cm^{-1} in FTIR spectra of a phytolith (Puppe and Leue, 2018), Sipernat 320 (precipitated silica, Evonik, Germany), and Aerosil 300 (a pyrogenic silica; Evonik, Germany) adapted from Ellerbrock et al. (2022).

groups ending at the surfaces that will be saturated by H forming of Si-OH groups (Farmer, 1974; Van der Marel and Beutelspacher, 1976).

The differences in the intensity of the band at approximately 800 cm^{-1} (Figures 3A, 4) are in accordance with Banerjee (1993) who stated that the shape and intensity of the peaks at 800 to 780 cm^{-1} in the IR/FTIR spectra change gradually from quartz to Libyan glass (Gucsik et al., 2004) or artificial glasses (Laudisio et al., 1998) as the crystallinity decreases in the sequence quartz > chalcedony > opal-CT > opal-A >> Libyan dessert glass.

Our data of amorphous inorganic silica fit into this sequence. The band at approximately 1,600 cm^{-1} in FTIR of Sipernat 300 (Figure 4) and phytolith (Figure 4) indicates the presence of water within the crystalline structure of these samples, caused by synthesis: precipitation in aqueous solution. The WN of the δ Si-O-Si band maxima in the spectra of Sipernat and Aerosil (799–805 cm^{-1}) are in a similar range as that of bASi (800 cm^{-1}; Table 3), suggesting similarities in the crystallinity.

Differences in the band intensities (*Y*-axis) indicate in general differences in the contents of the respective functional groups but are also affected by an extinction coefficient which is characteristic for the studied components [Lambert–Beers law; Hesse et al. (2005)]. Adapting the procedure that uses FTIR spectra to quantify the quartz concentration in the air of working places according to DGUV-213-582-2016 (2015) may therefore allow estimating the proportion of different Si species in solid mixtures. However, without knowing the extinction coefficients of a certain sample, it is difficult to use the absorbance values (*Y*-axis) for quantification purposes. Alternatively, the intensity of the ν Si-O band at WN 1120 to 1,000 cm^{-1} can potentially be used as an internal reference since for all studied Si species, it was the most intense band in the FTIR. Such an intensity ratio between the δ Si-O_{quartz} band and ν Si-O band may reflect the relative quartz content in a quartz-phytolith mixture (Figure 5).

For this alternative, the heights of the ν Si-O and ν Si-O-Si (quartz) band maxima can be calculated as a measure of the band intensity using IR analytical software (e.g., Bio-Rad Winirez Bio-Rad Corp., Krefeld, Germany). Specifically, the height of the band

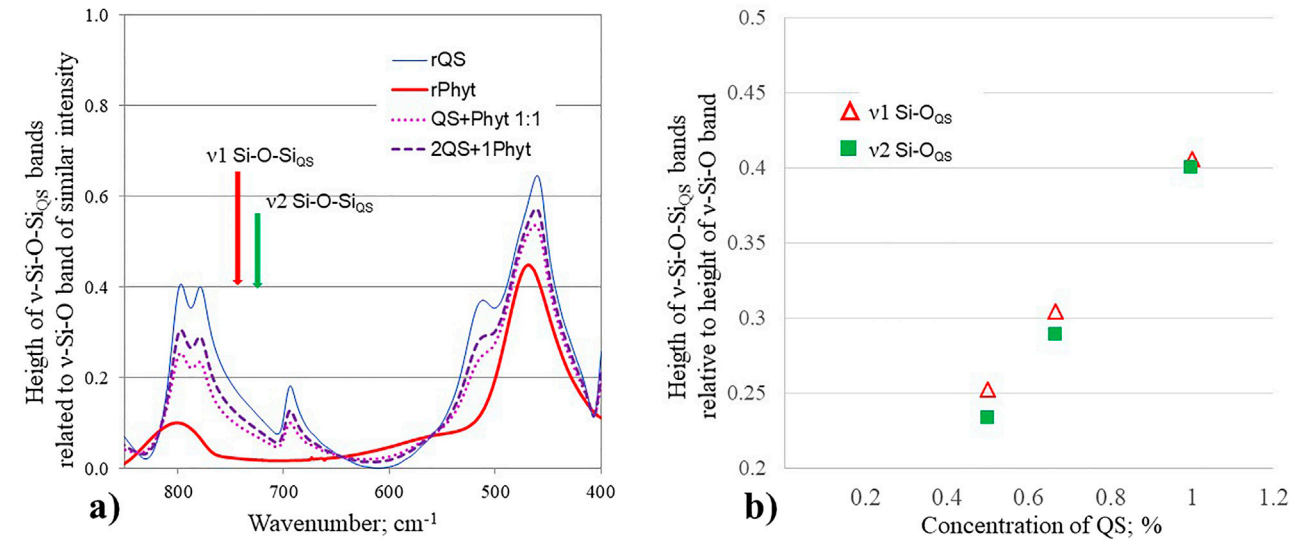

FIGURE 5
(A) FTIR at WN 850 to 400 cm^{-1} of quartz, Sipernat, and 1:1 as well as 1:2 phytolith and quartz-phytolith mixtures (dotted lines) showing the δ Si-O_{phyt} and δ Si-O_{quartz} bands with their intensities relative to that of the ν Si-O band at 1,100 cm^{-1} and **(B)** height of those bands relative to that of the ν-Si-O band.

maxima for these bands is measured as the vertical distance from the peak of the band to the global baseline (Kaiser et al., 2008) within the regions specified in Table 2. Comparison of FTIR spectra of phytoliths and quartz (Figure 3A) indicates that the WN regions of the ν Si-O band are nearly identical. FTIR of phytolith–quartz mixtures indicate that the intensity of the quartz-derived ν Si-O-Si band (ν Si-O-Si_{quartz} band) relative to that of the ν Si-O band at WN 1100 decreases (Figure 5A) with increasing proportion of phytoliths in the mixture, which is related to the relative content of QS in the mixture (Figure 5B). Of course, for any of the abovementioned alternatives that may be useable for estimation of Si species different in crystallization, the applied calibration procedures need to be adapted for each of the Si-O species and need to be tested by analyzing mixtures of known composition.

4 Conclusion

FTIR serves as a powerful method to distinguish silica species based on their crystallinity. Our findings demonstrate that FTIR can effectively identify distinct spectral features associated with amorphous and crystalline silica, highlighting the relationship between silica structure and its spectral profile. The non-destructive nature of FTIR offers significant advantages over traditional wet chemical methods, allowing for accurate and repeated analyses of silica samples. This capability is particularly valuable in soil science, where understanding the silica composition is essential for assessing soil health and ecological responses. In this study, we focused on the qualitative analysis of silica species and their crystallinity using FTIR. While our findings provide a solid foundation for distinguishing between amorphous and crystalline silica, future research is needed to explore the quantitative aspects of silica analysis. Establishing reliable quantification methods will enhance our understanding of the abundance and distribution of different silica forms in various matrices. Moreover, it remains unclear whether silica can be accurately quantified in complex samples such as soil. The interactions of silica with other soil components may complicate the quantification process.

Data availability statement

The original contributions presented in the study are included in the article/Supplementary Material; further inquiries can be directed to the corresponding author.

Author contributions

RE: Conceptualization, Formal Analysis, Investigation, Methodology, Validation, Visualization, Writing–original draft, Writing–review and editing. MS: Conceptualization, Writing–original draft, Writing–review and editing. JS: Conceptualization, Writing–review and editing.

Funding

The author(s) declare that no financial support was received for the research, authorship, and/or publication of this article. The study received no funding.

Conflict of interest

The authors declare that the research was conducted in the absence of any commercial or financial relationships that could be construed as a potential conflict of interest.

Publisher's note

References

Banerjee, A. (1993). Notizen: investigation of the crystallinity of the modifications of silica by their IR-reflectance spectra. *Z. für Naturforsch. A* 48, 741–742. doi:10.1515/zna-1993-5-630

Christy, A. A. (2008). Quantitative determination of surface area of silica gel particles by near infrared spectroscopy and chemometrics. *Colloids Surfaces A Physicochem. Eng. Aspects* 322, 248–252. doi:10.1016/j.colsurfa.2008.03.021

DGUV-213-582-2016 (2015). "Method for the determination of quartz and cristobalite [air monitoring methods, 2015]," in *Pages 401-436 the MAK-collection for occupational health and safety: annual thresholds and classifications for the workplace* (Weinheim, Germany: WILEY-VCH Verlag GmbH and Co. KGaA).

Dietzel, M. (2002). "Interaction of polysilicic and monosilicic acid with mineral surfaces," in *Water-rock interaction*. Editors I. Stober and K. Bucher (Netherlands, Dordrecht: Springer), 207–235.

Ellerbrock, R., Höhn, A., and Rogasik, J. (1999). Functional analysis of soil organic matter as affected by long-term manurial treatment. *Eur. J. Soil Sci.* 50, 65–71. doi:10.1046/j.1365-2389.1999.00206.x

Ellerbrock, R., Stein, M., and Schaller, J. (2022). Comparing amorphous silica, short-range-ordered silicates and silicic acid species by FTIR. *Sci. Rep.* 12, 11708. doi:10.1038/s41598-022-15882-4

Ellerbrock, R. H., Gerke, H. H., and Deumlich, D. (2016). Soil organic matter composition along a slope in an erosion-affected arable landscape in North East Germany. *Soil Tillage Res.* 156, 209–218. doi:10.1016/j.still.2015.08.014

Farmer, V. C. (1974). The infrared spectra of minerals. *Mineral. Soc. Monogr.* 4, 331–363.

Fröhlich, F. (2020). The opal-CT nanostructure. *J. Non-Crystalline Solids* 533, 119938. doi:10.1016/j.jnoncrysol.2020.119938

Gottwald, W., and Wachter, G. (1997) "IR spectroscopy for practicioners," in *German: IR Spektroskopie für Anwender*. Weinheim, Germany: Wiley VCH.

Gucsik, A., Koeberl, C., Brandstätter, F., Libowitzky, E., and Zhang, M. (2004). Infrared, Raman, and cathodoluminescence studies of impact glasses. *Meteorit. and Planet. Sci.* 39, 1273–1285. doi:10.1111/j.1945-5100.2004.tb00946.x

Gunde, M. K. (2000). Vibrational modes in amorphous silicon dioxide. *Phys. B Condens. Matter* 292, 286–295. doi:10.1016/s0921-4526(00)00475-0

Haberhauer, G., and Gerzabek, M. (1999). Drift and transmission FT-IR spectroscopy of forest soils: an approach to determine decomposition processes of forest litter. *Vib. Spectrosc.* 19, 413–417. doi:10.1016/s0924-2031(98)00046-0

Hernández-Ortiz, M., Hernández-Padrón, G., Bernal, R., Cruz-Vázquez, C., and Castano, V. (2015). Nanocrystalline mimetic opals: synthesis and comparative

characterization vs. natural stones. *Int. J. Basic Appl. Sci.* 4, 238–243. doi:10.14419/ijbas.v4i2.4174

Hesse, M., Meier, H., and Zeeh, B. (2005). *Spektroskopische Methoden in der organischen Chemie*. Georg Thieme Verlag.

Ichikawa, A., Volpato, J., O'Donnell, G. E., and Mazereeuw, M. (2022). Comparison of the analysis of respirable crystalline silica in workplace air by direct-on-filter methods using X-ray diffraction and fourier transform infrared spectroscopy. *Ann. Work Expo. Health* 66, 632–643. doi:10.1093/annweh/wxab094

Ji, J., Ge, Y., Balsam, W., Damuth, J. E., and Chen, J. (2009). Rapid identification of dolomite using a Fourier Transform Infrared Spectrophotometer (FTIR): a fast method for identifying Heinrich events in IODP Site U1308. *Mar. Geol.* 258, 60–68. doi:10.1016/j.margeo.2008.11.007

Kaiser, M., Ellerbrock, R., and Gerke, H. (2008). Cation exchange capacity and composition of soluble soil organic matter fractions. *Soil Sci. Soc. Am. J.* 72, 1278–1285. doi:10.2136/sssaj2007.0340

Kaiser, M., Zederer, D. P., Ellerbrock, R. H., Sommer, M., and Ludwig, B. (2016). Effects of mineral characteristics on content, composition, and stability of organic matter fractions separated from seven forest topsoils of different pedogenesis. *Geoderma* 263, 1–7. doi:10.1016/j.geoderma.2015.08.029

Katz, O., Puppe, D., Kaczorek, D., Prakash, N. B., and Schaller, J. (2021). Silicon in the soil–plant continuum: intricate feedback mechanisms within ecosystems. *Plants* 10, 652. doi:10.3390/plants10040652

Laudisio, G., Catauro, M., Costantini, A., and Branda, F. (1998). Sol–gel preparation and crystallisation of 2.5 CaO· $2SiO_2$ glassy powders. *Thermochim. Acta* 322, 17–23. doi:10.1016/s0040-6031(98)00487-0

Liu, H., Kaya, H., Lin, Y. T., Ogrinc, A., and Kim, S. H. (2022). Vibrational spectroscopy analysis of silica and silicate glass networks. *J. Am. Ceram. Soc.* 105, 2355–2384. doi:10.1111/jace.18206

McMillan, P. F., and Piriou, B. (1983). Raman spectroscopic studies of silicate and related glass structure: a review. *Bull. Mineral.* 106, 57–75. doi:10.3406/bulmi.1983.7668

Meloni, P., Carcangiu, G., and Delogu, F. (2012). Specific surface area and chemical reactivity of quartz powders during mechanical processing. *Mater. Res. Bull.* 47, 146–151. doi:10.1016/j.materresbull.2011.09.014

Puppe, D., and Leue, M. (2018). Physicochemical surface properties of different biogenic silicon structures: results from spectroscopic and microscopic analyses of protistic and phytogenic silica. *Geoderma* 330, 212–220. doi:10.1016/j.geoderma.2018.06.001

Ren, X., Zhang, W., and Ye, J. (2017). FTIR study on the polymorphic structure of tricalcium silicate. *Cem. Concr. Res.* 99, 129–136. doi:10.1016/j.cemconres.2016.11.021

Schaller, J., Cramer, A., Carminati, A., and Zarebanadkouki, M. (2020). Biogenic amorphous silica as main driver for plant available water in soils. *Sci. Rep.* 10, 2424. doi:10.1038/s41598-020-59437-x

Schaller, J., Macagga, R., Kaczorek, D., Augustin, J., Barkusky, D., Sommer, M., et al. (2023). Increased wheat yield and soil C stocks after silica fertilization at the field scale. *Sci. Total Environ.* 887, 163986. doi:10.1016/j.scitotenv.2023.163986

Schaller, J., Puppe, D., Kaczorek, D., Ellerbrock, R., and Sommer, M. (2021). Silicon cycling in soils revisited. *Plants* 10, 295. doi:10.3390/plants10020295

Šimon, I., and McMahon, H. (1953). Study of the structure of quartz, cristobalite, and vitreous silica by reflection in infrared. *J. Chem. Phys.* 21, 23–30. doi:10.1063/1.1698615

Stein, M., Georgiadis, A., Gudat, D., and Rennert, T. (2020). Formation and properties of inorganic Si-contaminant compounds. *Environ. Pollut.* 265, 115032. doi:10.1016/j.envpol.2020.115032

Stein, M., Puppe, D., Kaczorek, D., Buhtz, C., and Schaller, J. (2024). Silicon extraction from x-ray amorphous soil constituents: a method comparison of alkaline extracting agents. *Front. Environ. Sci.* 12. doi:10.3389/fenvs.2024.1389022

Van der Marel, H. W., and Beutelspacher, H. (1976). *Atlas of infrared spectroscopy of clay minerals and their admixtures*. Elsevier Publishing Company.

Wilson, M. (2014). The structure of opal-CT revisited. *J. Non-Crystalline Solids* 405, 68–75. doi:10.1016/j.jnoncrysol.2014.08.052